Total Photonuclear Cross Sections for Low Atomic Number Elements

J. M. WYCKOFF, B. ZIEGLER,* H. W. KOCH, AND R. UHLIG†
National Bureau of Standards, Washington, D. C.
(Received 17 September 1964)

Total photonuclear cross sections have been measured in an attenuation experiment using a scintillation pair spectrometer and an x-ray spectrum with a fixed maximum energy of 90 MeV. The cross sections as a function of x-ray photon energy for beryllium, carbon, oxygen, sodium, magnesium, aluminum, silicon, sulfur, calcium, nickel, cobalt, copper, and silver show detailed structure in many cases at x-ray energies of 15–30 MeV and display a consistent trend in shapes and magnitudes. The integrated cross sections up to 35 MeV relative to the classical dipole sum rule show a monotonic increase with atomic weight. Other analyses of the total photonuclear cross sections in terms of mean energies and of the ratios of the total cross sections to photoneutron cross sections are also presented.

INTRODUCTION

BREMSSTRAHLUNG spectra with a fixed maximum energy of 90 MeV were attenuated by long attenuators in the present experiment. The energy distributions of the transmitted x-ray spectra were measured in a good geometry experiment[1] by means of a scintillation pair spectrometer that represents a good compromise between resolution and detection efficiency.[2] From an analysis of the voltage pulse-height distribution on the spectrometer output by either the center-of-response procedure,[3] or the iterative analysis technique[4] with and without the x-ray attenuator, total attenuation cross sections have been evaluated for a wide range of elements. The emphasis has been on broad energy and element coverage in order to provide a consistent and relatively accurate determination of the total attenuation cross sections. Calculated total electronic cross sections were subtracted from the measured total cross sections to provide the photonuclear cross sections.

The cross sections for the electronic processes, such as pair production and Compton production, are slowly varying functions of energy and atomic number and can be calculated and justified to accuracies better than 1% in the 10–90-MeV range. In contrast, the total photonuclear cross sections are rapidly varying in energy and atomic number and are not known in most cases to better than 20% accuracy. To provide some perspective on these cross sections, the nuclear cross section for carbon-12 at the peak energy of the giant resonance of 22.5 MeV is 8.5% of the total electronic cross section. Also, the integrated nuclear cross section from 20 to 80 MeV is only 1% of the total integrated electronic cross sections.

Previous determinations of total photonuclear cross sections have employed magnetic spectrometers, either of the Compton[5] or pair[6] types, with a limited number of elements and energies, but with x-ray energy resolutions better than 2%. Other determinations have used scintillation spectrometers with energy resolutions about 10% on only five elements: carbon, oxygen, aluminum, sulfur, and iron.[1] Measurements made with variable energy gamma rays from the $T(p,\gamma)$ reaction are available in the energy range from 20.0 to 21.2 MeV.[7]

Total photonuclear cross sections can and have been synthesized from photoproton and photoneutron cross sections but with discouraging results for low atomic number elements because of the inconsistency of methods, because of incomplete coverage of the elements, and because of incomplete theoretical information of what to expect of the various component photonuclear cross sections. For elements above copper, the information on total photonuclear cross sections is, in general, good since these cross sections are obtainable from the photoneutron cross sections. A good understanding of the photonuclear reactions for high atomic number elements has thus resulted from photoneutron experiments[8] and from the hydrodynamical calculations of Danos and Greiner[9] and Okamoto.[10]

The results of the present experiment are presented by describing the general experimental procedure, the data analysis, the evaluation of uncertainties, the experimental results, and a discussion of the results. An appendix presenting a calculation on effective level

---

* Guest worker at the National Bureau of Standards from 1960–1962, on leave from the Nuclear Physics Section, Max Planck Institute for Chemistry, Mainz, Germany.

† Present address: University of Maryland, College Park, Maryland.

[1] J. M. Wyckoff and H. W. Koch, Phys. Rev. **117**, 1261 (1960), and J. Kockum and N. Starfelt, Nucl. Instr. Methods **5**, 37 (1959).

[2] B. Ziegler, J. M. Wyckoff, and H. W. Koch, Nucl. Instr. Methods **24**, 301 (1963).

[3] B. Ziegler, private communication and Natl. Bur. Std. (U. S.) Technical Note (to be published).

[4] R. Uhlig, J. Res. Natl. Bur. Std. **68A**, 401 (1964).

[5] J. Dular, G. Kernel, M. Kregar, M. V. Mihailović, G. Pregl, M. Rosina, and Č. Zupančič, Nucl. Phys. **14**, 131 (1959).

[6] N. A. Burgov, G. V. Danilyan, B. S. Dolbilkin, L. E. Lazareva, and F. A. Nikolaev, Zh. Eksperim. i Teor. Fiz. **43**, 70 (1962) [English transl.: Soviet Phys.—JETP **16**, 50 (1962)]; B. Ziegler, Z. Physik **152**, 566 (1958); Nucl. Phys. **17**, 238 (1960).

[7] E. E. Carroll, Jr. and W. E. Stephens, Phys. Rev. **118**, 1256 (1960).

[8] E. G. Fuller and Evans Hayward, *Nuclear Reactions* (North-Holland Publishing Company, Amsterdam, 1962), Chap. II, p. 113, and E. Ambler, E. G. Fuller, H. Gerstenberg, and R. S. Kaeser, Bull. Am. Phys. Soc. **7**, 461 (1962).

[9] M. Danos, Bull. Am. Phys. Soc. **1**, 246 (1956); Nucl. Phys. **5**, 23 (1958); M. Danos and W. Greiner, Phys. Rev. **134**, B284 (1964).

[10] K. Okamoto, Progr. Theoret. Phys. (Kyoto) **15**, 75 (1956); Phys. Rev. **110**, 143 (1958).

widths is referred to in the discussion and should be useful in interpreting the results.

Results for the elements carbon, oxygen, magnesium, aluminum, silicon, sulfur, and calcium have been obtained with good statistics and are detailed in this paper for x-ray energies of 10–35 MeV. Additional results for magnesium, aluminum, and calcium in the energy range of 35–70 MeV are presented. Results obtained by the same techniques but with poorer statistics for the elements beryllium, sodium, cobalt, nickel, copper, and silver are also given.

EXPERIMENTAL PROCEDURE

The determination of a total attenuation cross section consisted in the measurements of the x-ray spectra without and with a single length of a specific attenuator. The geometry, source of x-rays, and general operating conditions were the same as described previously.[1]

The changes in the present experiment were in the pulse-height analyzer, spectrometer, and the detailed control of the operating conditions.[2]

The x-ray spectra incident on the attenuator were fixed 90-MeV maximum bremsstrahlung, distorted by either zero, 165.8, or 331.8 grams per cm^2 of lithium. The filtration introduced by the lithium served to shape the pulse-height distribution so that the largest number of counts per channel was recorded in the channels near the peak of the giant photonuclear resonance. The required length of the filter or distorter varied for the range of elements studied because of the systematic variation in the electronic attenuation cross sections. The attenuator lengths were the maximum lengths that allowed the highest permissible x-ray detection rate by the scintillation pair spectrometer of 1.4 x-ray photons per synchrotron burst with the peak operating x-ray intensity from the synchrotron. Thus the counting rate was approximately 300 000 counts per hour.

Once having settled on the appropriate attenuator and operating conditions, the data leading to normalized counts in each of the 256 channels of the pulse-height analyzer were taken. The counts were normalized to a unit charge of an x-ray transmission monitor. The usual total counting time per spectrum per attenuator was two days. This time was subdivided into individual runs of four hours that were preceded and succeeded by standard calibration procedures described in detail in the spectrometer paper.[2] These checks permitted a monitoring of any spectrometer or analyzer gain changes of more than 0.3%. Any change of more than 1% was used to reject a run. The data were measured in two types of experiments. In the first type, the relative shape of the transmitted spectrum was measured. In the second type, the measured quantity was the absolute total count per ionization charge. The shape runs were recorded at the rate of about 1.4 counts per synchrotron burst with a dead time loss of approximately 20%. The total spectrum counts per charge

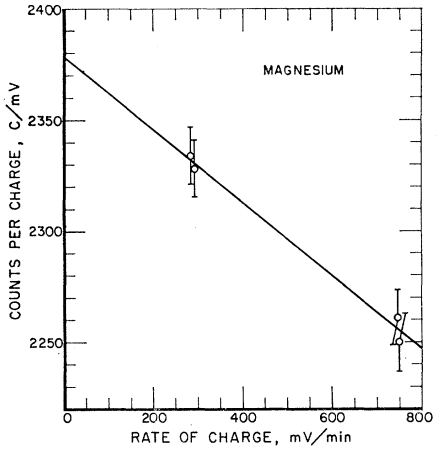

FIG. 1. Plot of the counts per unit charge versus count rate for magnesium. This is a typical case showing the means used to correct for the dead-time effect.

were obtained as a function of the ionization charge rate. The latter data were extrapolated to zero charge rate in order to correct for dead time loss as is illustrated in Fig. 1 for magnesium. The relative shape data up to the maximum count rates used were little affected by pile-up. This was shown with the technique described in the paper by Ziegler, *et al.*[2]

Table I lists the attenuator characteristics, the length of the lithium distorter, the total time per attenuator experiment, and the maximum photon energy recorded. All of the attenuators used had natural isotopic abundances. The maximum energy[11] is listed as either 45 or 90 MeV. The 45-MeV data were stressed in order to obtain statistically significant shapes for the pulse-height distributions in the 10–35-MeV range. The 90-MeV data were measured in order to provide a normalized pulse-height distribution produced by the complete energy range of the x-ray spectrum incident on the spectrometer and in order to obtain the absolute normalization factor for the 45-MeV data.

In order to define the detailed attenuation coefficients up to a photon energy of 45 MeV, the most critical data are the normalized 45-MeV pulse-height distributions measured both with the attenuator and without the attenuator. The procedure for obtaining these normalized distributions varied among the elements used and depended on whether the attenuator and distorter lengths were the same for the 45- and 90-MeV experiments. Accordingly, the elements as tabulated in Table I are subdivided into three categories. Category I are those attenuators for which the 90-MeV distributions were normalized directly from the total counts per charge data and then the 45-MeV distributions were normalized to the normalized 90-MeV distributions in the energy range from 35 to 40 MeV. This direct procedure was possible because the attenuator and

[11] These energies are nominal energies selected for convenience in identifying the runs.

TABLE I. Conditions for the experiment and data analysis.

Element	Density, g/cm³	Impurities and condition	45 MeV Attenuator length, g/cm²	45 MeV Distorter length, g/cm²	45 MeV Recording time, min	90 MeV Attenuator length, g/cm²	90 MeV Distorter length, g/cm²	90 MeV Recording time, min
Category I								
Magnesium	1.737	0.01% Al, 0.01% Fe 0.01% Ti	279.3	165.8	2273	279.3	165.8	78
Aluminum	2.688	a	267.3	165.8	2060	267.3	165.8	98
Calcium	1.533	0.44% Mg, 0.34% Al	211.6	165.8	1083	211.6	165.8	140
Cobalt	8.827	0.42% Ni	140.7	331.8	1330	140.7	331.8	121
Silver	10.476	<0.01%	104.6	331.8	832	104.6	331.8	164
Category II								
Beryllium	1.847	0.01% O, 0.08% C	496.1	0	1964	496.1	165.8	50
Carbon	1.70	graphite	496.4	0	1870	496.4	165.8	75
Oxygen	0.996	water	448.1	0	1766	373.8	165.8	461
Nickel	8.876	0.08% Co, 0.05% C, 0.07% Mg	133.2	331.8	913	159.7	165.8	137
Copper	8.905	...	141.2	331.8	1338	167.9	165.8	231
Category III								
Sodium	0.966	<1% Ca	245.0	0	1362	...	...	...
Silicon	2.329	polycrystalline	263.6	165.8	2251	...	...	...
Sulfur	1.931	crystalline	202.8	165.8	1068	...	...	...

[a] 1.2% Mg, 0.31% Fe, 0.1% Cu, 0.24% Cr, 0.64% Si—leading to 0.5% correction to measured cross section.

distorter lengths were the same for all of the experimental runs. These lengths were not the same for all of the elements, unfortunately, because of the lack of foresight of the present experimenters in the accumulation of the final data. Therefore, additional complications were introduced in the analysis of the data for the elements that fell into the following two categories:

Category II elements had a mixed normalization since the varying lengths of attenuator and distorter required corrections in order to derive a normalized 45-MeV distribution.

Category III elements had a normalization factor obtained from the criterion that the measured pulse-height distribution could be normalized to a predicted pulse-height distribution at energies below the particle emission thresholds. The prediction was obtained by attenuating the incident x-ray spectrum by the use of theoretical electronic attenuation coefficients, and by folding into this spectrum the spectrometer response function matrix. The factor had to be evaluated from the predicted pulse-height distribution because the 90-MeV pulse height distributions were not measured for the elements in this category.

DATA ANALYSIS

The total nuclear cross section $\sigma(\gamma,\mathrm{Tot})$ has been calculated by subtracting from the measured total cross section $\sigma_T(k)$ the calculated total electronic cross section $\sigma_e(k)$:

$$\sigma(\gamma,\mathrm{Tot})_k=\sigma_T(k)-\sigma_e(k)-\Delta\sigma_{\mathrm{arb}}, \quad (1)$$

where the arbitrary normalizing constant $\Delta\sigma_{\mathrm{arb}}$ will be discussed later. The measured quantity, $\sigma_T(k)$, may be expressed with proper normalizing factors in the following form:

$$\sigma_T(k)=\{\ln[N_0/N]_k\}/\rho x$$
$$=\{\ln[u(P_0)/u(P)]+\ln F_0-\ln F\}/\rho x, \quad (2)$$

where ρx is the density ρ times length x for the attenuator cm^{-2}; N_0,N are the incident and transmitted number of photons, respectively, at the photon energy k in an energy interval Δk in the x-ray spectrum; P_0,P are the pulse-height distributions produced by the x-ray spectra transmitted by the distorter alone and by the attenuator and distorter, respectively, in units of counts per channel per total distribution counts; F_0,F are the normalization factors for the pulse-height distributions, P_0 and P, respectively, in units of total distribution counts per ionization chamber charge in millivolts times the chamber capacitance; u is the symbol for the unfolding operator, as developed by Uhlig[4] that converts a pulse-height distribution into a photon number spectrum.

The calculated quantity, $\sigma_e(k)$, may be expressed as a sum of partial cross sections with their attendant corrections:

$$\sigma_e(k)=\sigma_{\mathrm{pair}}+\sigma_{\mathrm{triplet}}+\sigma_{\mathrm{Compton}}$$
$$=(\sigma_p+\Delta\sigma_p)+(\sigma_t+\Delta\sigma_t)+(\sigma_C+\Delta\sigma_C). \quad (3)$$

The quantities in this equation are discussed in more detail elsewhere[12] but are summarized here.

[12] H. W. Koch, Nucl. Instr. Methods 28, 199 (1964).

1. Electron-pair production in the field of the nucleus σ_p.

(a) Unscreened cross sections: Calculations of this cross section for nonscreened nuclei were made using Bethe-Ashkin's[13] formula 110, originally derived by Bethe and Heitler.[14]

(b) Screening corrections: The screening correction was based on the form factor obtained from the Hartree self-consistent field model.[15] An interpolation procedure was used to provide screening corrections for those elements for which the Hartree form factor was not available.

(c) Coulomb corrections: The Coulomb correction applied to the pair cross sections was basically that derived by Davies, Bethe, and Maximon.[16] However, improvements in their correction were derived by slight theoretical and experimental modifications described in another paper[12] in which several typographical errors appear. The improved Coulomb correction is the additive cross section $\Delta\sigma_{pC}$ given by

$$\Delta\sigma_{pC}=(Z/137)^4\times(1/E_k)[C_1+C_2\ln E_k+C_3(\ln E_k)^2],$$

where E_k = photon energy in MeV divided by 0.51 MeV and

$$C_1=-966.3\text{ b},$$
$$C_2=+804.3\text{ b},$$
$$C_3=-125.1\text{ b}.$$

2. Electron-pair production in the field of the atomic electrons σ_t (triplet production). The triplet cross section was calculated using the formula of Borsellino[17] corrected for atomic binding.[18,19]

3. Compton scattering, σ_C. The cross sections for this process were calculated by the Klein-Nishina formula for free electrons as tabulated in NBS Circular 583.[20]

4. Radiative corrections, $\Delta\sigma$. The total radiative corrections to the cross sections were assumed to be zero. However, after the present results and paper were in final form Mork and Olsen[21] were able to derive the radiative corrections. They find that the radiative correction to pair and triplet production at very high energies is the constant percentage of 0.9% which is independent of atomic number and reasonably independent of photon energy. Although this correction will be zero at the pair production threshold, it is probably a good assumption that the correction is +0.9% at the giant resonance energies around 20 MeV. These authors find that the correction to the total Compton cross section is a smoothly varying function of 0.32% at 10 MeV, 0.45% at 20 MeV, 0.56% at 30 MeV, 0.65% at 40 MeV, 0.73% at 50 MeV, 0.79% at 60 MeV, and 0.85% at 70 MeV. The influences of the radiative corrections on the present results will be discussed below.

The integral of $\sigma(\gamma,\text{Tot})_k$ has been obtained from a simple numerical integration to 35 MeV of Eq. (1) to give Σ_{35}

$$\Sigma_{35}=\int_0^{35}\sigma(\gamma,\text{Tot})_k dk \tag{4}$$

which has been plotted as a ratio to the classical sum rule expression, Σ_c

$$\Sigma_c=60(NZ)/A\text{ MeV-mb}. \tag{5}$$

The one arbitrary factor $\Delta\sigma_{\text{arb}}$ used in obtaining the total photonuclear cross section deserves special discussion to explain how it was obtained. In the next section the magnitude of this quantity relative to measurement and calculational uncertainties is discussed. To obtain $\Delta\sigma_{\text{arb}}$ the added requirement was placed on the $\sigma(\gamma,\text{Tot})$ that at a reasonable reaction threshold energy, the cross section $\sigma(\gamma,\text{Tot})_{k\text{thresh}}$ is equal to zero. For those elements included in category III of the Experimental Procedure section, there could be no separation of $\sigma_T(k)$ and $\Delta\sigma_{\text{arb}}$, due to the fact that the normalizing factors F and F_0 were not measured for these elements. For beryllium the $\Delta\sigma_{\text{arb}}$ was obtained by an evaluation of the expected nonzero cross section at 10 MeV.

EVALUATION OF UNCERTAINTIES

The uncertainties owing to possible systematic errors, statistics on measured quantities, and the limited accuracy in the theoretical calculations will be discussed in this section.

Systematic Errors

The uncertainties in the measured quantity $\sigma_T(k)$ will first be discussed in terms of the right-hand side of Eq. (2). From this equation the errors that enter directly can be seen to relate to the attenuator characteristics ρx three aspects of which may be considered:

(a) Density and length. The condition of each attenuator and the corrections for effective densities where required are noted in the discussion section. Errors in the density and length values cause $\sigma_T(k)$ to be multiplied by a constant. Since σ_e is assumed to be known, these errors have the effect of both shifting and distorting the photonuclear cross section. However, the distortion will be a smooth function of photon energy. These sources of error were found to be small.

[13] H. A. Bethe and J. Ashkin, *Experimental Nuclear Physics*, edited by E. Segre (John Wiley & Sons, Inc., New York, 1953), Vol. I, 1st ed., pp. 326, 327.
[14] H. A. Bethe and W. Heitler, Proc. Roy. Soc. (London) **A146**, 83 (1934).
[15] A. T. Nelms and I. Oppenheim, J. Res. Natl. Bur. Std. **55**, 53 (1955).
[16] H. Davies, H. A. Bethe, and L. C. Maximon, Phys. Rev. **93**, 788 (1954).
[17] A. Borsellino, Helv. Phys. Acta **20**, 136 (1947); Nuovo Cimento **4**, 112 (1947).
[18] H. A. Bethe and J. Ashkin, *Experimental Nuclear Physics*, edited by E. Segre (John Wiley & Sons, Inc., New York, 1953), Vol. I, 1st ed. p. 260.
[19] J. A. Wheeler and W. E. Lamb, Jr., Phys. Rev. **55**, 858 (1939).
[20] G. White Grodstein, Natl. Bur. Std. (U. S.) Circ. 583 (1957).
[21] K. J. Mork and H. A. Olsen (private communication).

TABLE II. Uncertainties for category I and II elements.

Element	Statistical uncertainty: Unattenuated spectrum (%)	Statistical uncertainty: Attenuated spectrum (%)	Statistical uncertainty: Counts per charge (mb)	Statistical uncertainty: Combined effect (mb)	Normalization: Energy MeV	Normalization: $\Delta\sigma_{arb}$(mb) (no rad. cor.)	Normalization: Rad. Cor. (mb)	Normalization: $\Delta\sigma_{arb}$(mb) (with rad. cor.)
Category I								
Magnesium	0.75	1.1	± 1.37	± 2.7	15.0	4.00	5.56	−1.56
Aluminum	0.75	1.0	± 1.44	± 3.0	12.5	0.32	5.96	−5.64
Calcium	0.75	0.93	± 2.60	± 5.3	12.5	4.52	12.3	−7.76
Cobalt	1.6	0.90	± 5.10	±17.5	10.0	18.0	18.5	−0.5
Silver	1.6	0.98	±15.2	±44.8	9.0	119.5	46.8	62.7
Category II								
Beryllium	0.75	0.90	± 0.25	± 0.5	10.0	2.51	0.99	1.52
Carbon	0.75	0.85	± 0.33	± 0.7	15.0	2.34	1.88	0.46
Oxygen	0.75	0.60	± 0.36	± 1.2	12.5	5.00	2.77	2.23
Nickel	0.75	0.85	± 6.1	± 9.3	11.5	1.43	21.2	−19.8
Copper	0.75	0.65	± 4.7	± 9.6	10.0	6.00	20.9	−14.9

(b) Purity and condition of the attenuator. The purity and condition of the attenuators is discussed separately for each case in the next section. In the few cases where impurities were significant, it was decided that an adequate correction could be made by changing the effective value of ρx.

(c) Geometry (inscattering corrections). Calculations and a separate experiment to determine the magnitude of any possible inscattering corrections showed that the corrections due to imperfect geometry were small. Therefore, no corrections have been made.

Uncertainties in the energy assignment for Eq. (2) may lead to a distortion of the derived cross section dependent both on energy and atomic number. Considerable effort was made, as described in the spectrometer paper of Ziegler *et al.*,[2] to reduce the energy uncertainty to ±1%. No corrections have been applied to the cross section as a result of this uncertainty.

Statistical Uncertainties

The statistical uncertainties arise for each of the quantities in the curly brackets of Eq. (2), F_0, F, and the pulse-height distributions, P_0 and P.

The normalization factors F_0 and F lead to a simple cross section displacement of the total cross section independent of photon energy. The errors in this displacement arise from two sources: the uncertainties due to the counts per charge measurement are shown in column 3 of Table II and the uncertainties associated with the normalization of the 45-MeV data to the 90-MeV data are shown in columns 1 and 2. The combined uncertainties are shown in column 4.

The statistical uncertainties in the original pulse-height analyzer counts are somewhat magnified by the iterative unfolding technique leading to uncertainties at individual energies. The enhancement factor a_0 given in Uhlig's paper[4] varies from 1.5 to 3.1. Statistical uncertainties obtained in this way are drawn at three energies on each of the photonuclear cross section plots.

Calculational Uncertainties

The systematic errors entering into the calculation of the electronic cross section can only be guessed at. However, if there are no compensating errors, a comparison with accurately measured cross sections below the photonuclear threshold and well above the energy region where photonuclear cross sections are expected to be large, can give some confirmation of the calculations.

It is perhaps of value to show the small, radiative correction to the pair cross section as a separate column 7 in Table II with the threshold energy at which the correction was calculated in column 5. When this correction is applied to $\sigma_e(k)$ a small residual cross section at threshold remains, as is listed in column 8. With this large sensitivity to small electronic cross-section corrections it is perhaps surprising that the arbitrary correction is so small, and in one-third of the cases within the statistical uncertainty shown in column 4. The magnitude of the residual correction before the radiative correction has been applied is shown in column 6. It is this $\Delta\sigma_{arb}$ that has been applied to category I and II elements.

The small radiative corrections may be used to point out the inherent uncertainty in the photonuclear cross section integrated over energy above 35 MeV as is shown in Figs. 14, 16, and 22 for magnesium, aluminum, and calcium. The dot-dash line indicating a corrected baseline results from these corrections. The corrections over-correct and suggest a negative cross section in magnesium and calcium, which is a physical impossibility. Both refined measurements and refined calculations of the pair and triplet cross sections above 35 MeV may be required to throw light on this uncertain region. Below 35 MeV the corrections are relatively much less important and the measured cross sections integrated over energy are consequently more significant.

RESULTS

The results of the experiment are presented for each element in (a) uncorrected pulse-height distributions, Figs. 2 and 3, for the 45-MeV runs; (b) total nuclear cross sections, either in 125- or in 500-keV energy bins or both; and (c) integrated nuclear cross sections obtained by integrating the fine grid data up to a given x-ray energy. The points on the cross section plots are always the results of the present experiment.

The total photonuclear cross sections are given in the 10–35-MeV energy range in Figs. 4, 6, 8, 11, 13, 15, 19, 21, 23, 25, 27, and 29. A smooth, solid line representing the best estimate of the results of the present experiment is drawn on the figure on which is given the 500-keV data points. The lines drawn on the figures presenting the 125-keV data points are always the results of other experiments, which are provided for comparison with the present results. These other data are either other total photonuclear cross sections, or photoneutron cross sections. The comparisons are provided to be illustrative only. No attempt was made to be comprehensive in the examination of previous data. Each figure showing total-cross-section points has also shown three error bars to illustrate the magnitude of the statistical uncertainties discussed in the previous section. Also shown on each total-cross-section figure is a curved baseline (dot-dashed curve) that demonstrates the effect on the photonuclear cross section of a 0.9% increase in the pair and triplet cross sections and the appropriate 0.3–0.8% increase in the Compton scattering cross section.

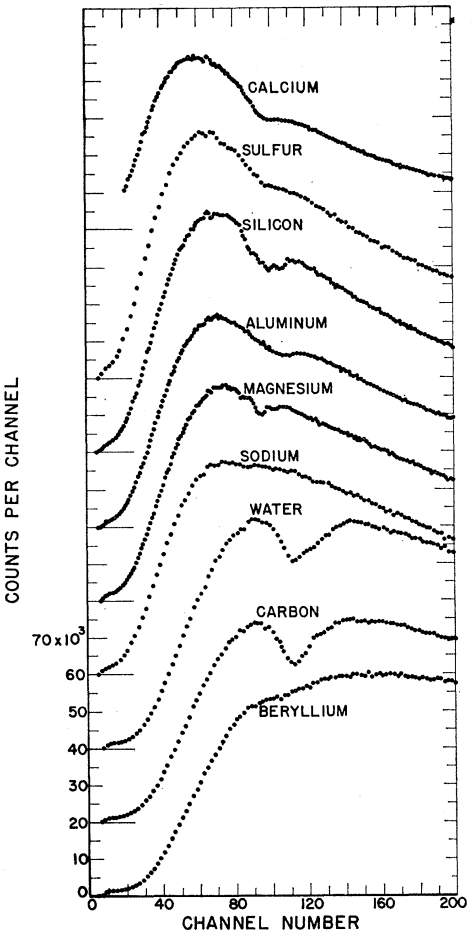

FIG. 2. Pulse-height distributions for nine elements. The information columns for 45 MeV in Table I apply to these data. Successive elements have been displaced by 20 000 counts per channel in order to separate these data.

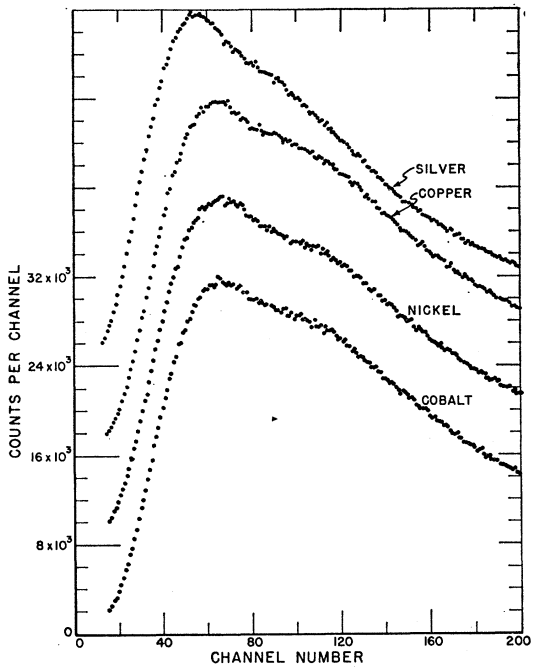

FIG. 3. Pulse-height distributions for four elements. Successive elements have been displaced by 8000 counts per channel in order to separate these data.

The integrated nuclear cross sections are given to an energy of 35 MeV for all elements and to 70 MeV for magnesium, aluminum, and calcium. The integrated cross sections Σ are expressed in units of MeV-mb on the left-hand ordinate scale and in a ratio relative to the integrated cross section obtained from the classical dipole sum rule Σ_c as given in (Eq. 5), on the right-hand ordinate scale.

Each integrated-cross-section figure has shown two straight lines that provide estimates of the normalizing uncertainties in the present experiment. The solid line represents the possible cumulative error in the integrated cross section due to the statistical uncertainties in the normalization of the total-cross-section data discussed previously. The actual normalization of the total cross sections by the requirement of zero nuclear cross section below threshold is shown by the dashed line. The dot-dashed curved line represents the new baseline required if the total radiative correction is applied to the calculated electronic cross section.

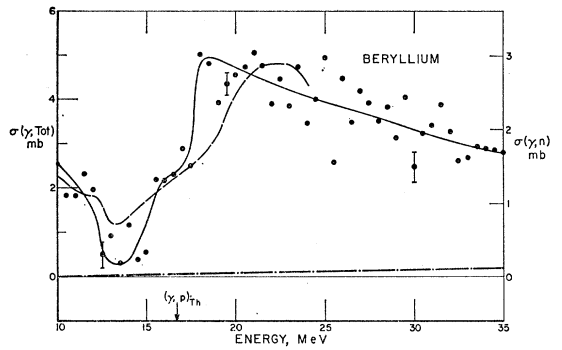

FIG. 4. Beryllium total photonuclear cross sections. The solid line is drawn as the best approximation to the experimental points using the left hand scale. The (γ,n) cross section obtained by Bertozzi *et al.* (Ref. 22) combined with that obtained by Nathan and Halpern (Ref. 23) is shown as a dashed line using the right-hand scale.

A. Beryllium

The beryllium attenuator consisted of two 2.34-cm-diam rods. For these rods, an activation experiment was performed using synchrotron x-rays to measure the possible impurities. Based on this experiment, only 0.01% oxygen and 0.08% carbon were detected. A spectroscopic analysis indicated no other significant impurities. The pulse-height distribution obtained with the beryllium attenuator in a 90-MeV x-ray spectrum is shown in Fig. 2.

The analysis of the pulse-height distribution up to 35 MeV resulted in the total photonuclear cross section

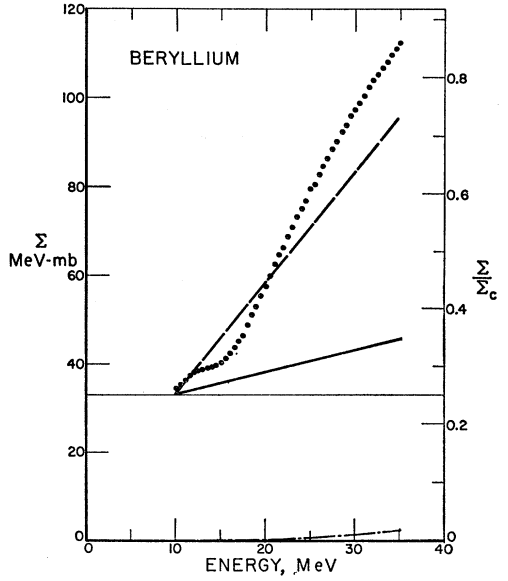

FIG. 5. Beryllium total photonuclear cross section integrated over energy. The points represent the experimental data. The solid line is the uncertainty in the baseline introduced by statistical considerations. The dashed line is the magnitude of baseline correction applied to bring the cross section to values measured by Bertozzi at 10 MeV. The dot-dashed line is the corrected baseline when the radiative correction is applied to the electronic cross section.

points in 500-keV energy bins given in Fig. 4. Since the beryllium nuclear cross section is small and distributed over a wide energy range, the statistical fluctuations are large and therefore only the 500-keV bin data are presented. For comparison with the present results (solid line), the photoneutron cross sections measured by Bertozzi *et al.*[22] in the 10–16-MeV region, and by Nathan and Halpern[23] in the 19–24-MeV region are combined and represented by the dashed line and the right-hand ordinate scale.

The integrated cross section for beryllium above 10 MeV is given in Fig. 5. However, because the photoneutron threshold is 1.6 MeV, not all of the integrated cross section up to a given photon energy is given by these results. It is estimated that the integrated cross section for beryllium from 1.6 to 10 MeV is 33-MeV-mb.

B. Carbon

The carbon attenuator consisted of 5-cm-diam graphite rods. As described in the paper by Wyckoff and Koch,[1] a variation in density with radial position in the rod required a 1% correction in the cross section data. The pulse-height distribution obtained with the carbon attenuator is shown in Fig. 2.

The total photonuclear cross section for carbon in 125-keV bins is shown in Fig. 6a and in 500-keV bins is shown in Fig. 6b. The solid curve drawn for comparison with the 125-keV bin data points in Fig. 8a are those obtained for $\sigma(\gamma,\mathrm{Tot})$ at the Lebedev Institute.[24] The curve has been drawn through their experimental points and has been shifted up in energy by 250 keV. Similar required shifts for other elements will be noted below and are within the estimated errors in the energy calibration which are 1% at 20 MeV.[2]

The integrated cross section for carbon is shown in Fig. 7. As will be noted, the normalization shift applied to the present total photonuclear cross sections for carbon (as shown by the dashed straight line) was larger than allowed by the estimated uncertainties (as shown by the solid straight line) in normalization. This result was found also for oxygen, another element in category II, and can be attributed to the effect of nonlinearities in the energy calibration of the 90-MeV data which affected the analysis of category II elements, but which did not affect the category I element analyses. The fact that different lengths of attenuator were used in the 90- and 45-MeV runs (see the description of the category II elements in Table I) made it necessary not only to normalize the 45-MeV data to the 90-MeV data, but also to calculate the effects of the differing attenu-

[22] W. Bertozzi, P. T. Demos, S. B. Kowalski, F. R. Paolini, and C. P. Sargent, *Proceedings of the International Conference on Nuclear Structure*, edited by D. A. Bromley and E. W. Vogt (University of Toronto Press, Toronto, 1960), p. 746, and private communication via E. G. Fuller.

[23] R. Nathan and J. Halpern, Phys. Rev. 92, 940 (1953).

[24] N. A. Burgov, G. V. Danilyan, B. S. Dolbilkin, L. E. Lazareva, and F. A. Nikolaev, Institute for Theoretical and Experimental Physics Circ. No. 146 Moscow, 1963 (unpublished).

ator lengths. This calculation is very sensitive to any small errors in the assignment of energy to the unfolded photon number spectrum and will lead to a large error in the normalization. For example, at 10 MeV, a 100-keV shift leads to a 2.3-mb shift in cross section. Fortunately, the procedure followed in the present experiment of normalizing the total nuclear cross sections to zero below the particle thresholds eliminates the effect of the normalization error for category II elements.

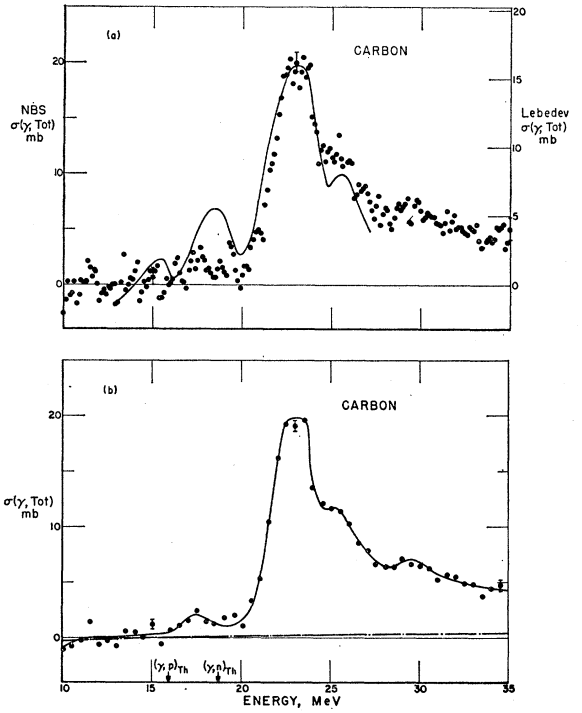

FIG. 6. Carbon total photonuclear cross section. Points on plots (a) and (b) represent the data of this experiment. The solid line drawn in (a) is the total photonuclear cross section obtained by the Lebedev group using the right-hand ordinate. For ease in comparing the shapes their data has been moved up in energy by 250 keV. The solid line in the lower plot (b) is drawn as the best approximation to the experimental points. The dot-dashed line represents the corrected baseline when the radiative correction is applied to the electronic cross section.

C. Oxygen

The oxygen results were obtained with long 2-in.-diam aluminum tubes filled with distilled water as the attenuator. The necessary corrections for temperature were applied to the tube and the water. The electronic attenuation cross section subtracted from the total measured cross section included the calculated hydrogen cross-section contribution. The 45-MeV pulse-height distribution obtained with a water attenuator is shown in Fig. 2.

The total photonuclear cross-section data points for oxygen are given in 125-keV bins in Fig. 8(a) and in

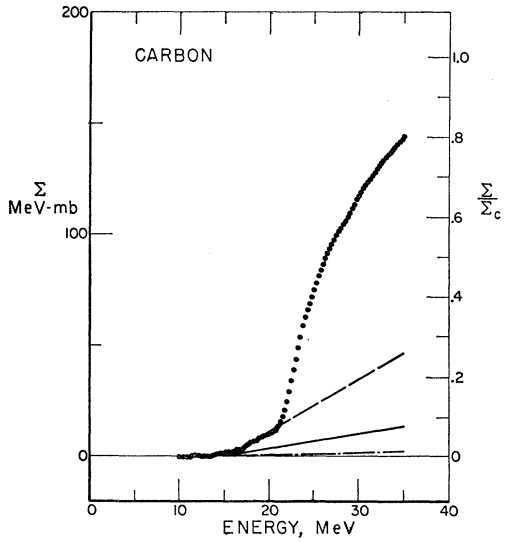

FIG. 7. Carbon total photonuclear cross section integrated over energy. The dashed line is the normalization applied to bring the cross-section values to zero at threshold.

500-keV bins in Fig. 8b. The final results for the present experiment are given in the curve of Fig. 8b.

The curve drawn on Fig. 8a represents the photo-

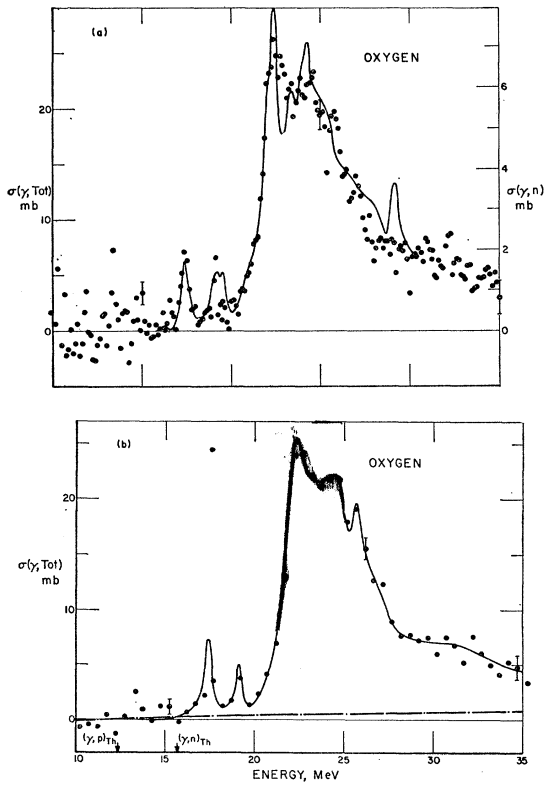

FIG. 8. Oxygen total photonuclear cross section. The Livermore photoneutron cross section represented by the solid line in (a) has been shifted up in energy by 250 keV.

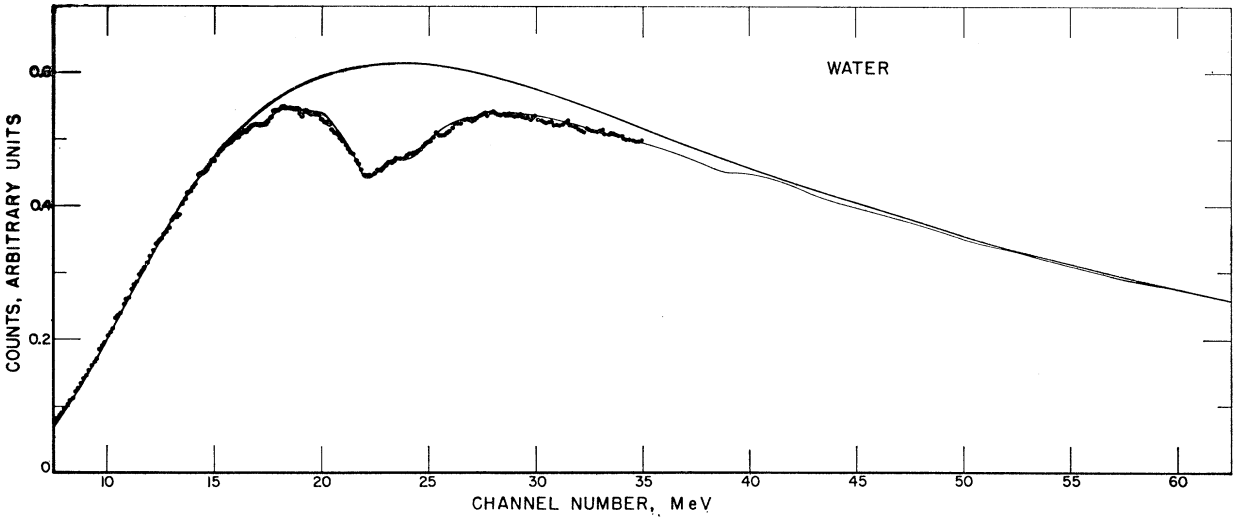

FIG. 9. Pulse height distribution for the water attenuator of Fig. 8. The top solid line is the calculated pulse-height distribution when the total photonuclear cross section is set equal to zero. The lower solid line is the calculated pulse-height distribution when the shape of the $\sigma(\gamma,n)$ measured by Anderson *et al.* (Ref. 26) is taken to be the $\sigma(\gamma,\text{Tot})$ shape with the magnitude normalized to fit the pulse-height distribution at the giant peak. The calculated cross section was moved up in energy by 250 keV to fit the measured shape.

neutron cross section data of the Livermore group[25] shifted up in energy by 250 keV. As will be noted, there is reasonably close agreement between the shapes of the two cross sections (total and photoneutron) below 28 MeV. The peak in the Livermore data at 28.9 MeV is not seen in the present results. A comparison between the left- and right-hand ordinate scales shows that the present total cross sections for oxygen are 3.7 times the photoneutron cross sections found at Livermore.

Because of the very considerable interest in the cross section structure reported for oxygen at energies above 30 MeV,[26] a special calculation was made, using the response-function matrix for the scintillation pair spectrometer to generate an expected pulse-height distribution to be obtained for the water attenuator and for a total cross section with a shape given by the Iowa State photoneutron cross section shape. The bottom solid line resulting from this prediction is shown to be in excellent agreement with the measured pulse-height-distribution data points as shown in Fig. 9. The photoneutron cross-section values were increased by a factor of 2.47 for this calculation and were shifted up in energy by 250 keV. The top line of this figure represents the pulse-height distribution to be expected for the water attenuator if there were no nuclear absorption in oxygen. The present experiment did not provide sufficiently good data (not presented here) for comparison in the very interesting 35–60-MeV region.

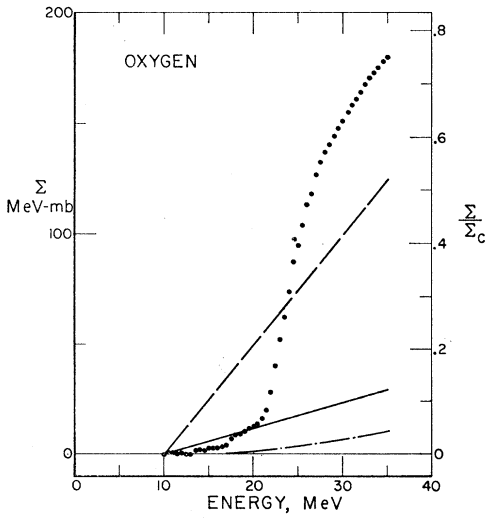

FIG. 10. Oxygen total photonuclear cross section integrated over energy.

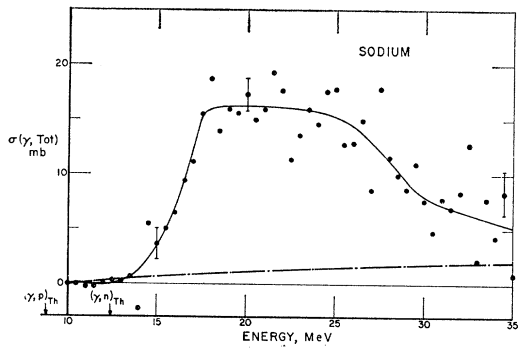

FIG. 11. Sodium total photonuclear cross section.

[25] R. L. Bramblett, J. T. Caldwell, and S. C. Fultz, Bull. Am. Phys. Soc. 8, 120 (1963); R. L. Bramblett, J. T. Caldwell, R. R. Harvey, and S. C. Fultz, Phys. Rev. **133**, B869 (1964).

[26] D. Anderson, A. Bureau, B. Cook, J. Griffin, J. McConnell, and K. Nybo, Phys. Rev. Letters **10**, 250 (1963).

The integrated cross sections for oxygen are given in Fig. 10.

D. Sodium

The sodium sample was prepared by melting the metal in an inert atmosphere and allowing it to solidify in a glass tube 3.0 cm in diameter. Corrections were made for the thin glass end window. The top surface of the metal was cut smooth. However, because bubbles formed along the glass wall, the density is uncertain by about 2%. For this reason the absolute sodium-cross-section data were obtained directly from the assumption that the cross section must be zero at the threshold for particle emission and did not result from a direct normalization of the sodium pulse-height distribution shown in Fig. 2. Therefore, no estimate of a normalization error is given on the integrated cross-section curve. This curve resulted from an integration of the data on the coarse grid results for sodium plotted in Fig. 11. The integrated cross section is given in Fig. 12.

E. Magnesium

The magnesium data were taken in two parts with an intervening pulse-height-analyzer baseline shift of seven channels out of 256 channels. The shift was introduced in order to test the possible introduction of fine structure by the analyzer. However, within the statistical errors, the two uncorrected pulse-height distributions were identical. Therefore, the two halves of the experimental runs on magnesium were corrected for the shift, summed, and plotted as the 45-MeV pulse-height distribution for magnesium shown in Fig. 2.

The total photonuclear cross section for magnesium has been plotted in 125-keV bins in Fig. 13(a). Also shown on this figure is a curve that is the total cross section measured for magnesium by the Lebedev group.[27] No cross-section normalization was applied in plotting their curve. However, the Lebedev data has been shifted up in energy by 375 keV in order to compare the shapes in more detail. As will be noted, the absolute cross sections resulting from the two experiments at the peaks agree reasonably well in contrast to the poorer agreement for the carbon cross sections shown in Fig. 6. The Lebedev magnesium result shown here goes to zero at 30 MeV. More recent Lebedev results[27] are in closer agreement with the results of the present experiment. The results of this experiment, grouped in 500-keV bins, are shown in Fig. 13(b).

The integrated cross section for magnesium is given from 10 to 70 MeV in Fig. 14. Note that the data are very poor statistically above 40 MeV, which is an indication of the poorer data obtained in the present experiment from the 90-MeV runs. This loss in quality is expected from the shorter experiment times listed in Table I.

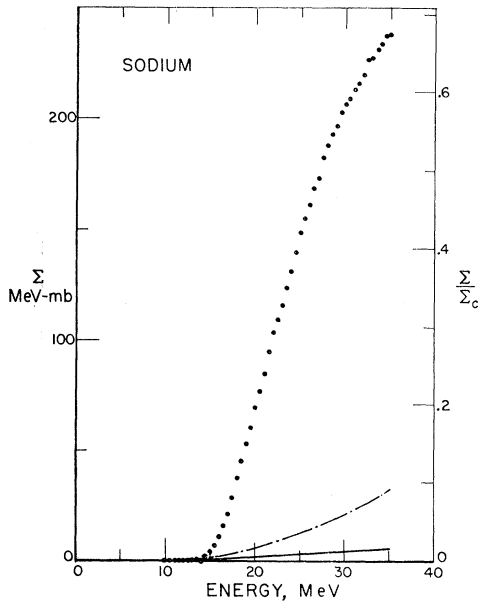

FIG. 12. Sodium total photonuclear cross section integrated over energy.

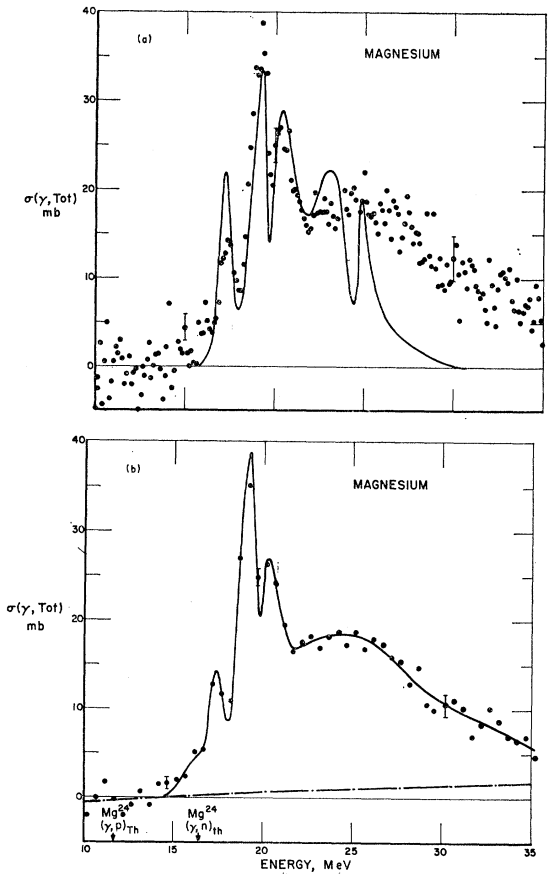

FIG. 13. Magnesium total photonuclear cross section. The solid line in (a) represents the Lebedev data moved up in energy by 375 keV.

[27] F. A. Nikolaev (private communication).

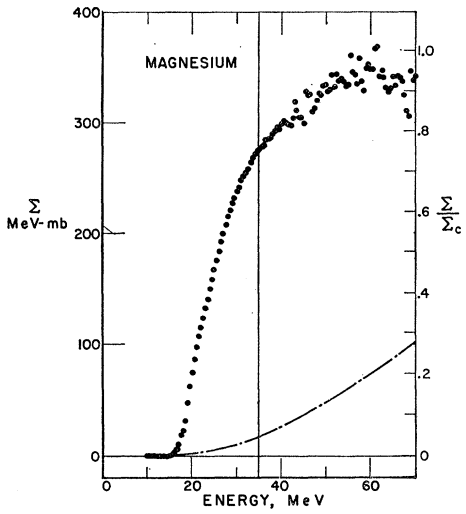

FIG. 14. Magnesium total photonuclear cross section integrated over energy. The dot-dashed line represents the corrected baseline resulting from the introduction of the calculated radiative corrections to the electronic cross sections.

F. Aluminum

The pulse-height distribution obtained with the aluminum attenuator shown in Fig. 2 was measured with the number of counts per channel comparable to the magnesium data of Fig. 2. Therefore, it is to be noted that the aluminum nuclear absorption dip in the pulse-height distribution has no evident structure in the 10–35-MeV region in contrast to the magnesium dip. Corrections were made for the rather large impurities in the aluminum samples that were itemized in Table I.

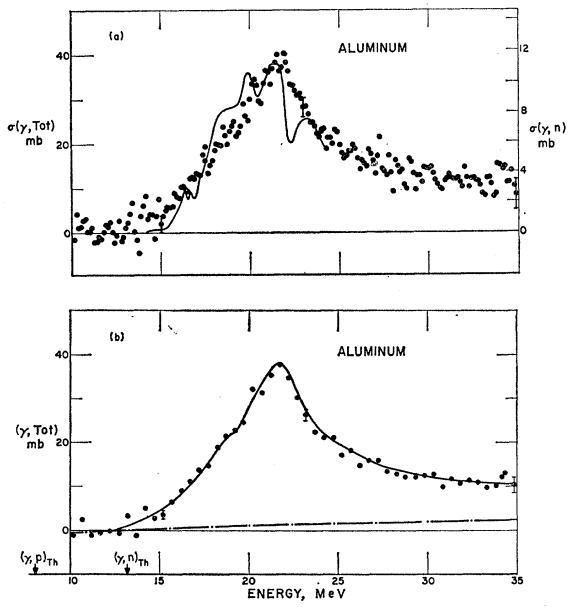

FIG. 15. Aluminum total photonuclear cross section. The solid line on (a) represents the $\sigma(\gamma,n)$ data of Spicer (Ref. 28) shifted up in energy by 250 keV using the right-hand ordinate scale.

The total cross section for aluminum is plotted in 125-keV bins in Fig. 15(a) and in 500-keV bins in Fig. 15(b). Figure 15(a) also shows the photoneutron cross section measured by Spicer[28] shifted up in energy by 250 keV.

The integrated cross section shown in Fig. 16 was plotted to 70 MeV. It may be noted from the dashed line of this figure that very little change in normalization was required to force the nuclear cross section to zero at threshold.

G. Silicon

The uncorrected pulse-height distribution, obtained with the silicon attenuator and plotted in Fig. 2, shows considerable fine structure.

The total photonuclear cross section for silicon has been plotted in 125-keV bins in Fig. 17(a) and in 500-keV bins in Fig. 17(b). Also drawn on Fig. 17(a) are the photoneutron results of the Livermore group.[29] These results have been shifted up by 250 keV in order to permit a detailed shape comparison. As is evident from Fig. 17(a), their neutron formation cross section, $\sigma(\gamma,n)+\sigma(\gamma,2n)+\sigma(p,n)+\cdots$, has a shape almost identical to the total-cross-section shape from the present experiment.

The integrated cross sections from 10 to 35 MeV are plotted in Fig. 18.

H. Sulfur

The crystalline sulfur sample was prepared by melting powdered sulfur in a glass tube and allowing it to cool

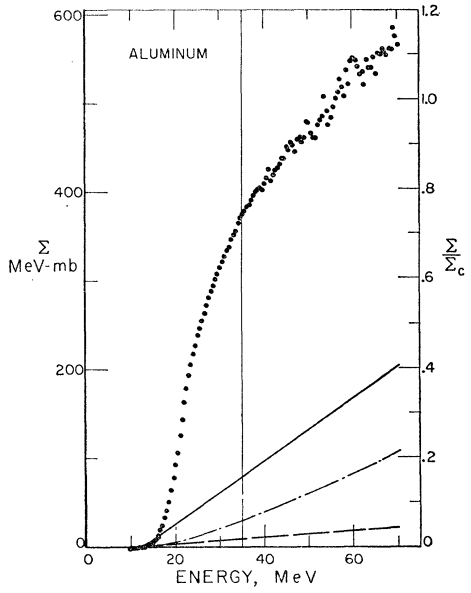

FIG. 16. Aluminum total photonuclear cross section integrated over energy. The solid line represents the baseline uncertainty due to statistical considerations. The dashed line represents the correction actually applied to normalize the photonuclear cross section to zero at 12.5 MeV. The dot-dashed line is the corrected baseline resulting from introduction of radiative corrections.

[28] B. M. Spicer (private communication).

[29] J. T. Caldwell, R. R. Harvey, R. L. Bramblett, and S. C. Fultz, University of California Radiation Laboratory Report No. UCRL 7424, 1963 (unpublished).

slowly. The end was then machined flat. However, due to the considerable density differences between the various crystalline forms of sulfur, the density could not be accurately measured. The pulse-height distribution obtained with the sulfur sample is shown in Fig. 2.

The total photonuclear cross section has been plotted in 125-keV bins in Fig. 19(a) and in 500-keV bins in Fig. 19(b). Also given on Fig. 19(a) are the total cross sections of the group at the Institut J. Stephan[5] which show striking differences from the present results.

The integrated cross sections from 10 to 35 MeV are plotted in Fig. 20.

I. Calcium

The calcium metal was obtained in the form of a large billet which was sliced lengthwise into four pieces. After x-ray examination of these pieces, the two pieces were used that showed the least density uncertainties due to blow holes produced in the casting. Corrections were applied for the aluminum and magnesium impurities. The pulse-height distribution obtained with the calcium attenuator is shown in Fig. 2.

The total-cross-section results for calcium are plotted in 125-keV bins in Fig. 21(a) and in 500-keV bins in Fig. 21(b). Also shown on Fig. 21(a) are the photoneutron cross sections of Baglin and Spicer,[30] which have been shifted up by 250 keV. The general shape of the $\sigma(\gamma,n)$ and the $\sigma(\gamma,\mathrm{Tot})$ seem to be the same up to 30 MeV.

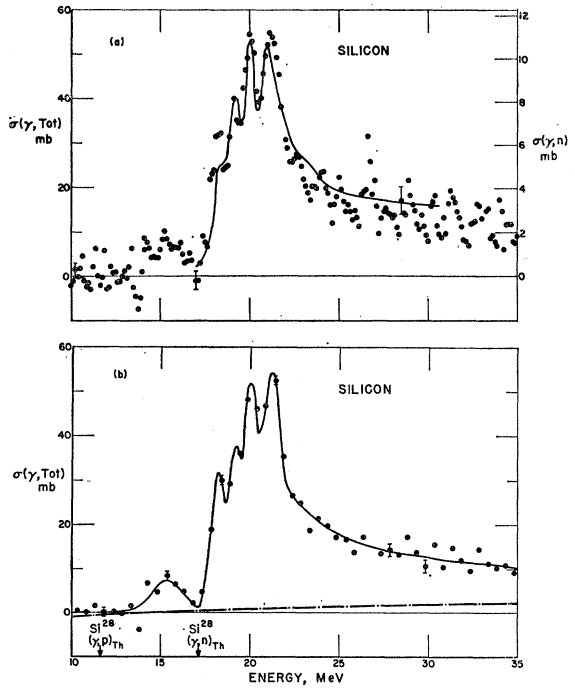

FIG. 17. Silicon total photonuclear cross section. The solid line on (a) represents the $\sigma(\gamma,n)$ data from the Livermore group shifted up in energy by 250 keV using the right-hand ordinate scale.

[30] J. E. E. Baglin and B. M. Spicer (private communication); and University of Melbourne Report No. UM-P-63/13, 1963 (unpublished).

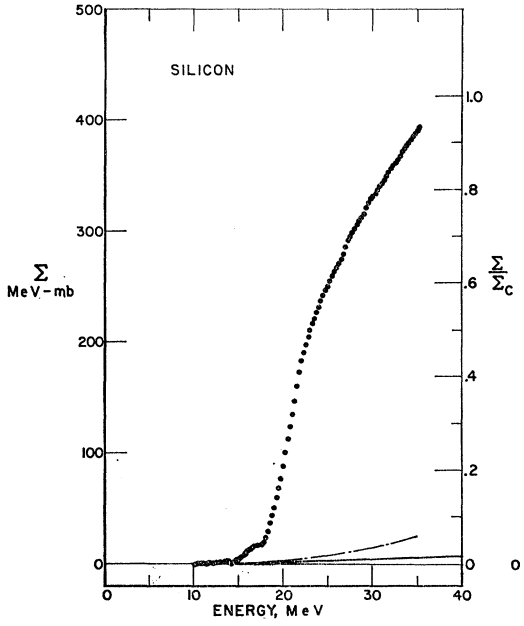

FIG. 18. Silicon total photonuclear cross section integrated over energy.

The integrated cross section has been plotted up to 70 MeV in Fig. 22 and seems to flatten off abruptly above 35 MeV. The normalization required to force the total cross section to be zero below the particle thresh-

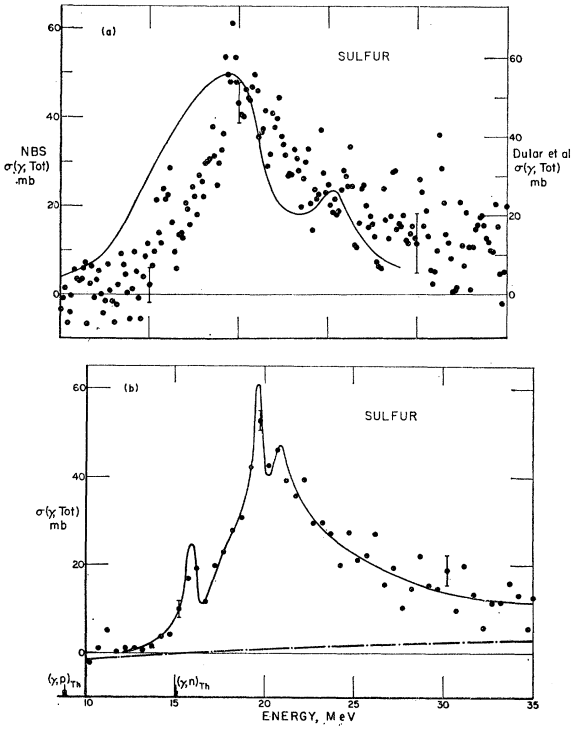

FIG. 19. Sulfur total photonuclear cross section. The solid line on (a) represents the $\sigma(\gamma,\mathrm{Tot})$ data of Dular *et al.* (Ref. 5) using the right-hand ordinate scale.

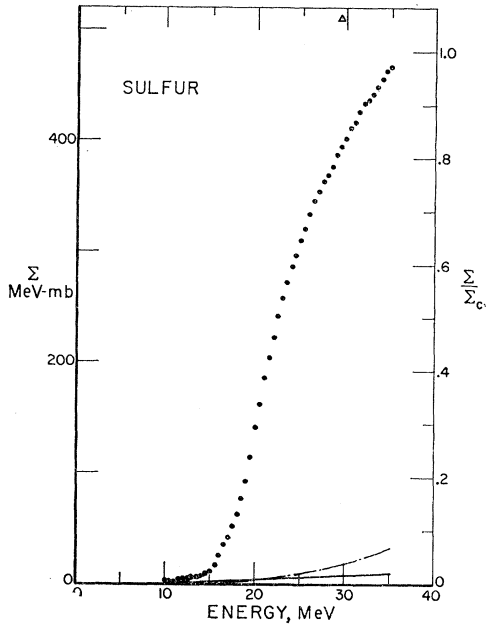

FIG. 20. Sulfur total photonuclear cross section integrated over energy.

olds (see dashed line) is within the statistical uncertainty in the normalization as shown by the solid line of Fig. 22.

J. Cobalt

The uncorrected pulse-height distribution measured with the cobalt attenuator is shown in Fig. 3. The total

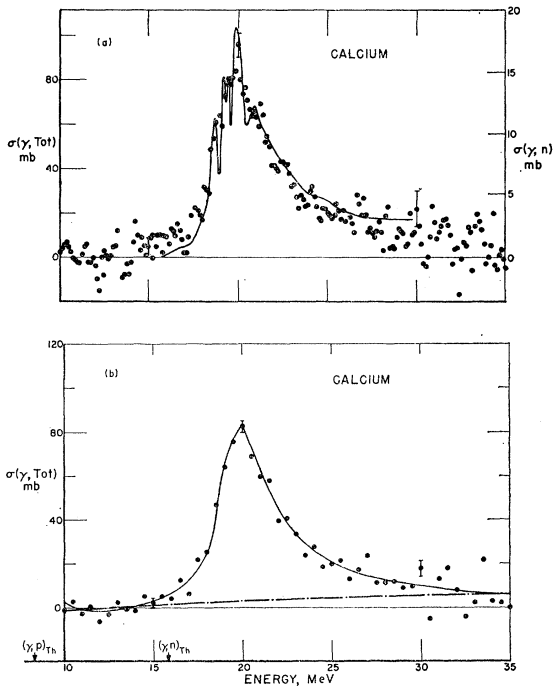

FIG. 21. Calcium total photonuclear cross section. The solid line in (a) represents the $\sigma(\gamma,n)$ data of Baglin and Spicer (Ref. 30) shifted up by 250 keV in energy using the right-hand ordinate scale.

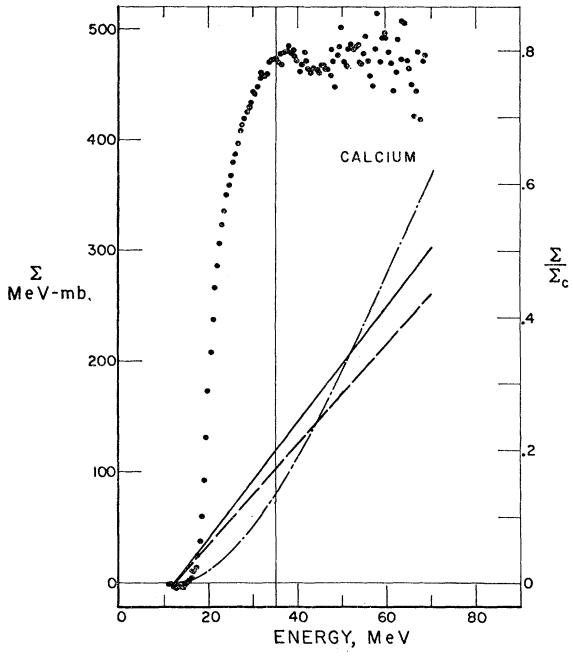

FIG. 22. Calcium total photonuclear cross section integrated over energy.

cross section obtained from an analysis of this distribution is given in 500-keV bins in Fig. 23. The solid line in this figure is the result of this experiment and the dashed line is the neutron formation cross section measured at Livermore.[31] The integrated cross section is shown in Fig. 24.

K. Nickel

The uncorrected pulse-height distribution is shown in Fig. 3; the total-cross-section results from this experiment are shown in Fig. 25; and the integrated cross sections for nickel are given in Fig. 26.

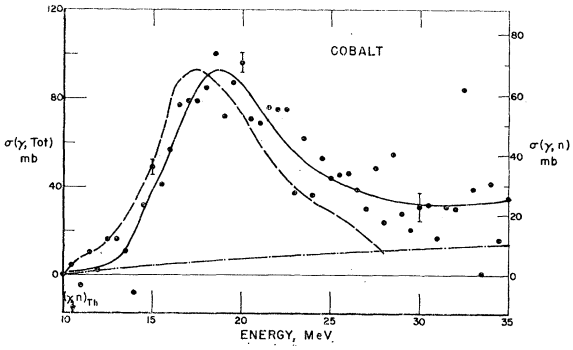

FIG. 23. Cobalt total photonuclear cross section. The solid line is drawn as the best approximation to the experimental points. The dashed line represents the $\sigma(\gamma,n)$ data of the Livermore group.

[31] S. C. Fultz, R. L. Bramblett, J. T. Caldwell, N. E. Hansen, and C. P. Jupiter, University of California Radiation Laboratory Report No. UCRL 6913, 1962 (unpublished).

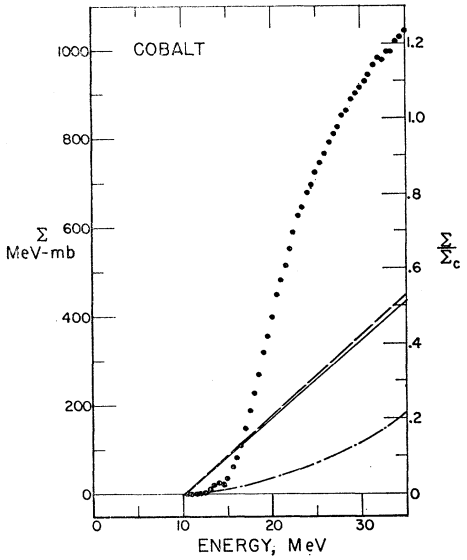

FIG. 24. Cobalt total photonuclear cross section integrated over energy. The solid, dashed, and dot-dashed lines have the same meaning as in Fig. 16.

L. Copper

The uncorrected pulse-height distribution is shown in Fig. 3; the total-cross-section results from this experiment are shown in Fig. 27; the integrated cross sections for copper are given in Fig. 28. Also shown on Fig. 27 (dashed curve) are the neutron-formation cross sections of the Livermore group.[32]

M. Silver

The uncorrected pulse-height distribution is shown in Fig. 3; the total-cross section results are shown in Fig. 29; the integrated cross sections for silver are given in Fig. 30. Also shown on Fig. 29 (dashed curve) are the photoneutron cross sections reported by Bogdankevich *et al.*[33]

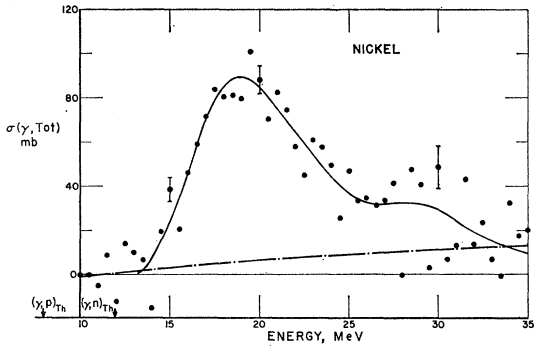

FIG. 25. Nickel total photonuclear cross section.

[32] S. C. Fultz, R. L. Bramblett, and J. T. Caldwell, Bull. Am. Phys. Soc. 8, 387 (1963).

[33] O. V. Bogdankevich, B. I. Goryachev, and V. A. Zapevalov, Zh. Eksperim. i Teor. Fiz. 42, 1502 (1962) [English transl.: Soviet Phys.—JETP 15, 1044 (1962)].

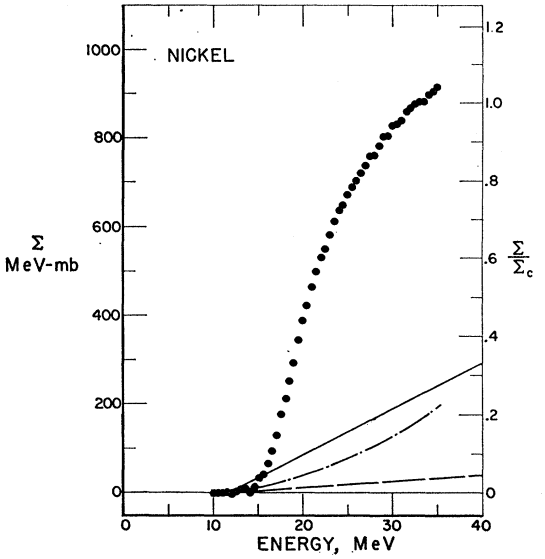

FIG. 26. Nickel total photonuclear cross section integrated over energy.

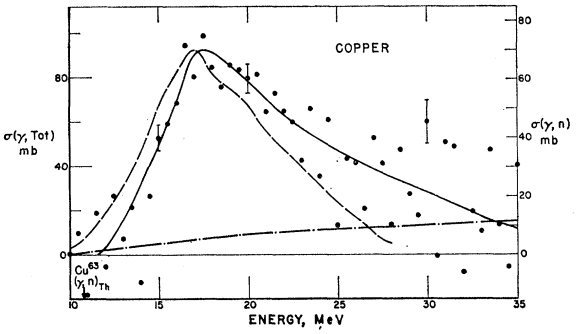

FIG. 27. Copper total photonuclear cross section. The dashed ine represents the $\sigma(\gamma,n)$ cross section of the Livermore group (Ref. 32) used with the right-hand ordinate scale.

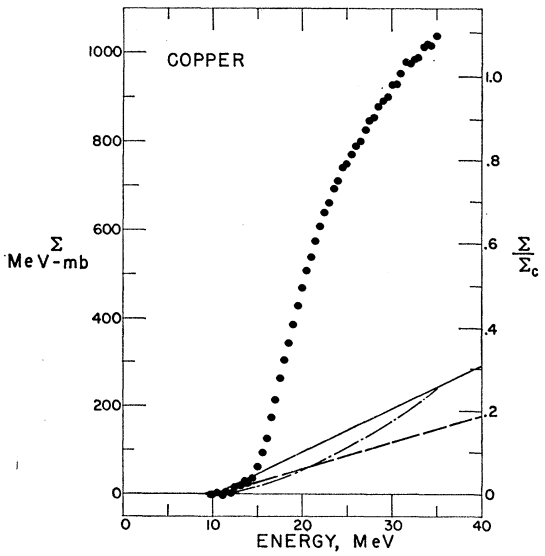

FIG. 28. Copper total photonuclear cross section integrated over energy.

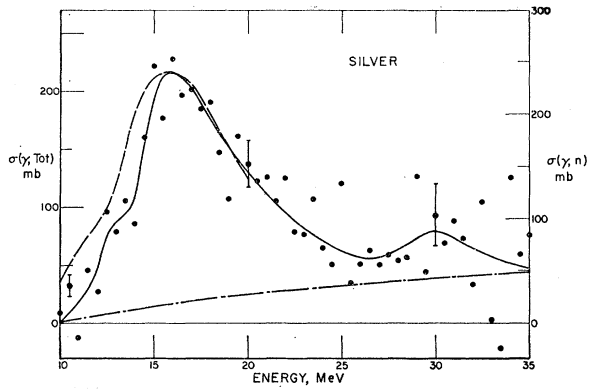

FIG. 29. Silver total photonuclear cross section. The solid line is drawn as the best approximation to the experimental points. The dashed line represents the $\sigma(\gamma,n)$ data of Bogdankevich *et al.* (Ref. 33) using the right-hand ordinate scale.

DISCUSSION OF RESULTS

Before presenting a summary and evaluation of the results presented in the last section, it would be desirable to provide some of the basic limitations of the use of a scintillation pair spectrometer in the measurement of total photonuclear cross sections. The following three limitations can serve as a guide to an evaluation of the data presented here.

(*a*) *Energy resolution.* The scintillation pair spectrometer is able to resolve cross-section-energy structure that is wider than 2% or 400 keV at 20 MeV. In addition, to the extent that the cross sections measured in this attenuation experiment are consistent with data measured by other methods, the level widths with which we are dealing must be greater than about 10 keV (see Appendix). Therefore, if other techniques indicate cross-section fine structure not observed here, that structure in the total photonuclear cross section must have widths between 10 and 400 keV.

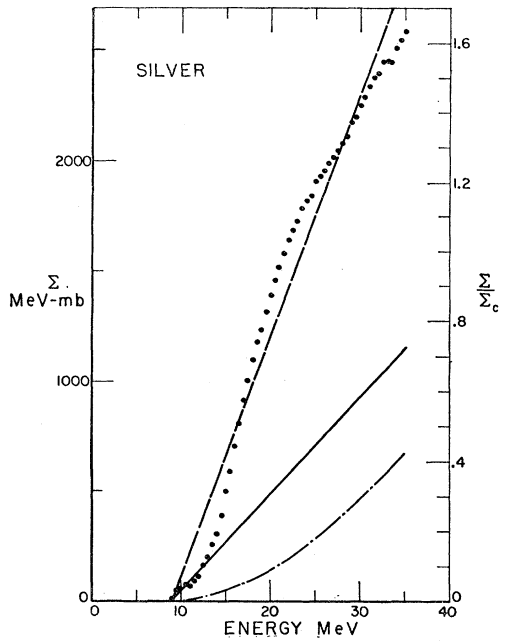

FIG. 30. Silver total photonuclear cross section integrated over energy.

The matrix used to unfold the response function from the cross section contained bins a minimum of 125-keV wide so that structure of 12-keV width, for example, would be reduced by a factor of about 10 due to this handling of the data alone. Structure 400-keV wide and wider would, within the statistics, be faithfully measured. The varying distortion introduced below 400-keV line widths can readily be inferred. Actually, the statistical limit was not trivial and, with the present number of counts, little more could have been learned if the spectrometer resolution had been improved.

(*b*) *Cross-section magnitudes.* The peak cross sections for wide resonances measured in this experiment should be reasonably accurate as shown in the section discussing the sources of error. However, the shapes of the high-energy tail of the total cross sections and the integrated cross sections measured in this experiment are very dependent on the adequacy of the electronic-cross-sections calculations. For example, a small variation in the calculated electronic cross sections could markedly influence the integrated cross sections as well as the high-energy-tail cross sections. This influence fortunately would be systematic and probably noticeable. The very fact that the triplet cross section is dependent on the first power of the atomic number (Z), as is the photonuclear cross section for such processes as quasideuteron production or higher order spallation, indicates the problem. Therefore, the present experiment has emphasized measurements on a wide range of elements. From an examination of the consistency of this wide range of elements, one can be assured of the reliability of the data on any one element.

(*c*) *Unseparated nuclides.* The requirement for long attenuators to amplify the effect of the nuclear absorption in the present experiment also requires that elements in their natural nuclidic composition be used. Therefore, if the fine structure which is characteristic of one nuclide is superimposed on the nuclear absorption of a neighboring nuclide, one can be assured that the result will be somewhat washed out. However, as can be seen from a comparison of the fine structure in magnesium and silicon and the lack of structure in aluminum, the change by one or two nucleons can destroy the fine structure resolvable for a nuclide by the present spectrometer. Therefore, it has been assumed that the fine structure found for even-even nuclides will be superimposed on a smoothly varying background for the neighboring-odd nuclide. If the odd nuclide is small in percentage composition, then the conclusion can indeed be drawn that the fine structure is almost completely attributable to the even-even nucleus.

With these limitations in mind, the results will be discussed in terms of the total photonuclear cross

sections, ratios of these cross sections to photoneutron cross sections, integrated total cross sections, harmonic mean and median energies, and the giant resonance width.

1. Total Photonuclear Cross Sections

The total photonuclear cross sections obtained from the present experiment and plotted in Figs. 4, 6, 8, 11, 13, 15, 17, 19, 21, 23, 25, 27, and 29 are perhaps best regarded as the total nuclear cross sections averaged over 500-keV bins. The total cross sections in these figures provide the data for the integrated cross sections, mean energy values, etc., given in Table III and the summary figures to follow.

The energy position of the principal cross-section structures for such elements as oxygen, magnesium, and silicon, and comparisons with other data discussed in the Results section, suggest that the energy assignment for all the data in the present experiment might be about 250 keV too high. This error is within the estimated error of the present experiment and has a negligible effect on the evaluation of the electronic and nuclear cross-section magnitudes for most elements at most energies. However, in the cases where the cross section is changing most rapidly with energy, reducing the energy assignment by 250 keV would introduce cross-section changes of nearly 10% of the photonuclear peak values. For example, for carbon at 15 MeV a change of -2 mb would be introduced and for silver at 35 MeV the change would be $+17$ mb.

The magnitudes of the total cross sections found in the present experiment are more internally consistent than total cross sections synthesized from previous photoneutron and photoproton cross sections or cross sections obtained from other total attenuation experiments. For example, the Lebedev group results for magnesium[24] are 33-mb peak at 19 MeV compared to the present data in Fig. 13 of 33 mb, whereas the Lebedev results for carbon[27] are 22-mb peak at 23.2 MeV compared to the present result in Fig. 6 of 19.8 mb. For sulfur, the Institut J. Stefan group[5] obtained 55 mb at 19.5 MeV compared to the present results in Fig. 19 of 61 mb at 19.6 MeV. Thus the comparisons are good and within the errors of the various experiments.

Similarly, the total cross sections synthesized from photoneutron and photoproton data are consistent with the present experiments. This general conclusion is interesting in view of the possible large influences of very fine structure in an attenuation experiment as discussed in the appendix. As shown in that discussion, the line width below which there would be an influence on the present results is about 10 keV. Since the present total cross sections for Si^{28} agree with synthesized values, Alles *et al.*,[34] who measured 6-keV-wide fine structure in $Al^{27}(p,\gamma)$, must have worked at the true line widths for Si^{28}.

[34] R. G. Alles, S. S. Hanna, L. Mayer-Schutzmeister, P. P. Singh, and R. E. Segel (to be published).

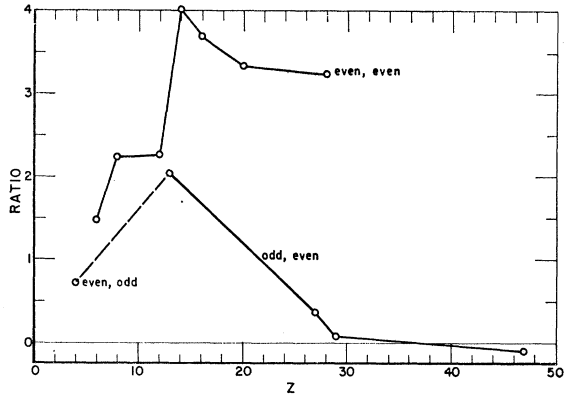

FIG. 31. The ratio, $[\sigma(\gamma,\mathrm{Tot})-\sigma(\gamma,n)]/\sigma(\gamma,n)$ versus Z. The descriptor represents the number of protons and then the number of neutrons.

2. Ratio of Total Cross Sections to Photoneutron Cross Sections

The detailed constancy of the ratio of total to photoneutron cross sections for Si^{28} up to 30 MeV is very striking in the data of Fig. 17(a). If the difference between the total and photoneutron cross sections is interpreted as the photoproton cross section, the silicon result indicates that the photoproton cross section relative to the photoneutron cross section is constant for Si^{28} over a wide energy range. This result is not in agreement with the prediction of Morinaga[35] who predicts ratios for $\sigma(\gamma,p)/\sigma(\gamma,n)$ at the peak of the giant resonance that are of the same magnitude as those found in the present experiment. However, his predictions would vary considerably over the 15-MeV range in which the $\sigma(\gamma,\mathrm{Tot})/\sigma(\gamma,n)$ is relatively constant in the present experiment. In order to investigate this result for other elements, this ratio minus 1 has been evaluated and plotted in Fig. 31 versus the atomic number. As can be seen from this figure, the ratio $[\sigma(\gamma,\mathrm{Tot})-\sigma(\gamma,n)]/\sigma(\gamma,n)$ increases with Z for the even-even nuclei to a peak value of 4.0 for Si^{28}.

The value of the Fig. 31 ratio for C^{12} is 1.5. This value has been successfully explained by Barker and Mann[36] as being due to the effects of isotopic-spin impurity mixing in the characteristics of the initial and final states. The studies of isotopic-spin impurities have been extended by MacDonald[37] for low-lying excited states. His predictions of less than 2 for the Si^{28} ratio of $\sigma(\gamma,p)/\sigma(\gamma,n)$ are only about half those required to explain the $[\sigma(\gamma,\mathrm{Tot})-\sigma(\gamma,n)]/\sigma(\gamma,n)$ ratios found in the present experiment just below the peak of the giant resonance.

[35] H. Morinaga, Phys. Rev. **97**, 444 (1955).
[36] F. C. Barker and A. K. Mann, Phil. Mag. **2**, 5 (1957).
[37] W. M. Macdonald, *Nuclear Spectroscopy*, edited by F. Ajzenberg-Selove (Academic Press Inc., New York, 1960), Part B, p. 932.

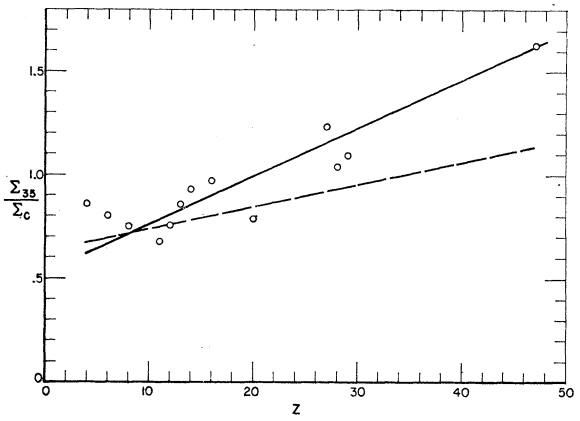

FIG. 32. The ratio of total photonuclear cross section integrated to 35 MeV, to the classical sum rule cross section integrated to 130 MeV is plotted versus Z. The upper solid line is drawn as the best straight-line fit to the experimental data. When radiative corrections are applied to the electronic cross sections the dashed line is the best fit to the new points (not shown).

3. Integrated Cross Sections

The right-hand ordinate of Figs. 5, 7, 10, 12, 14, 16, 18, 20, 22, 24, 26, 28, and 30 provides the integrated total cross section in units of the classical sum rule. The 35-MeV magnitude of these normalized integrated cross sections (without the radiative corrections) are given in Table III and in Fig. 32. These values show a slow monotonic increase in magnitude. Levinger[38] has derived the quasideuteron-cross-section expression which, when applied to photodeuteron cross-section data of Whalin *et al.*,[39] yields the integrated cross section

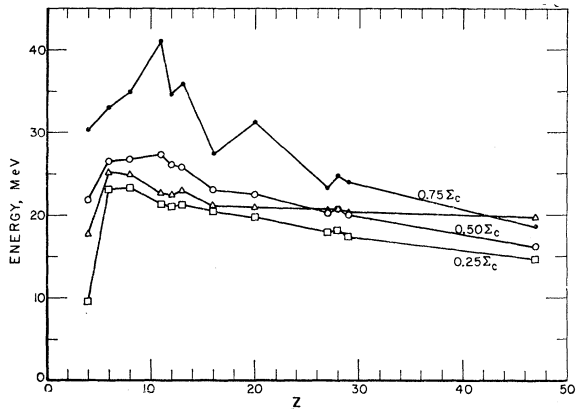

FIG. 33. Energies at points of special interest versus Z. The square points, open circle, and closed circle points represent the energies below which 25, 50, and 75% of the classical sum-rule cross section are found. The triangle points are the harmonic mean energies. These data are tabulated in Table III.

TABLE III. Cross-section summary data.

Element	Σ_σ (MeV-mb)	Σ_{35} (MeV-mb)	Energy (MeV) at $0.25\Sigma_c$	$0.50\Sigma_c$	$0.75\Sigma_c$	k_{peak}[a]	$\langle k \rangle$	σ_{peak} (mb)
Be	133.6	112.2	9.6	21.7	30.2	18.5	21.8	4.95
C	180.0	144.0	23.1	26.4	33.1	23.2	25.1	19.8
O	240.0	179.5	23.3	26.7	34.9	22.3	24.9	25.6
Na	344.3	239.0	21.2	27.2	40.7	19.3	22.7	16.2
Mg	364.7	276.0	20.7	26.0	34.6	19.2	22.4	32.6
Al	404.0	344.0	21.2	25.8	35.7	21.6	22.9	38.0
Si	420.9	391.0	20.3	23.0	29.1	21.2	23.0	54.0
S	480.9	466.0	19.6	22.4	27.4	19.6	21.1	61.0
Ca	600.6	472.0	19.7	22.4	31.2	20.0	20.9	83.0
Co	877.9	1042.0	17.8	20.2	23.2	18.7	20.7	93.0
Ni	878.5	912.0	18.2	20.7	24.8	18.9	20.7	89.0
Cu	946.2	1036.0	17.2	20.0	24.0	17.7	20.2	92.0
Ag	1591.4	2568.0	14.7	16.3	18.6	15.9	19.7	216.0

[a] Only values for the energy at which the maximum cross section occurs are listed; more detailed data can be taken from the individual data plots.

value from 35 to 150 MeV of

$$\int_{35}^{150} 6.3\frac{NZ}{A}\sigma_D dk = 1.12\left[0.06\frac{NZ}{A}\right] = 1.12\Sigma_c \text{ MeV-b}. \quad (6)$$

If the sum rule of Gell-Mann *et al.*[40] is used to calculate the total integrated cross section to the meson threshold, a value of $1.4\Sigma_c$ MeV-b is obtained. The difference between this sum and $1.12\Sigma_c$ should give the integrated sum from low energies to 35 MeV. However, this value of $0.28\Sigma_c$ is obviously too small in view of the experimental values in Fig. 32, which are all larger than $0.7\Sigma_c$. Therefore, the quenching[41] and reduction of the quasideuteron contribution to the sum rule in Eq. (6) is required to produce a total integrated sum to 150 MeV of $1.4\Sigma_c$. The amount of the quenching must vary with atomic number since the experimental cross-section sums to 35 MeV given in Fig. 32 vary with atomic number.

The influence of the radiative correction in decreasing the cross sections integrated to 35 MeV is shown by the dashed line of Fig. 32. Since the total cross sections for magnesium (Fig. 13) and calcium (Fig. 22) are made slightly negative at energies above 35 MeV, it would appear that the total electronic cross sections above 35 MeV relative to the cross sections at threshold energies has been slightly over-corrected by the addition of the radiative-cross-section corrections. Therefore, the true integrated-cross-section curve in Fig. 32 is expected to lie between the solid and dashed lines.

4. Harmonic Mean Cross Sections and Median Energies

The cross-section curves resulting from this experiment were used to generate harmonic mean cross

[38] J. S. Levinger, Phys. Rev. **84**, 43 (1951).
[39] E. A. Whalin, B. D. Schriever, and A. O. Hanson, Phys. Rev. **101**, 377 (1956).
[40] M. Gell-Mann, M. L. Goldberger, and W. E. Thirring, Phys. Rev. **95**, 1612 (1954).
[41] M. Danos, Bull. Am. Phys. Soc. 4, 102 (1959), and private communication.

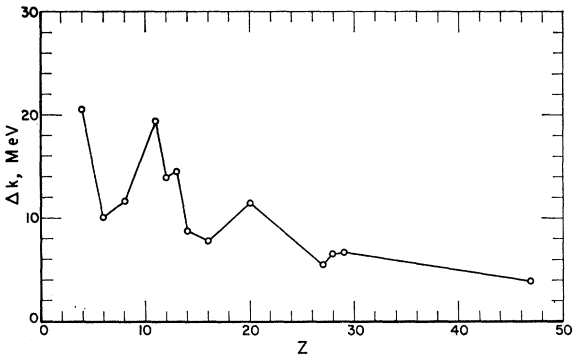

FIG. 34. The width of the giant resonance versus Z. The energy difference Δk between the 25% and 75% Σ_c values plotted in Fig. 33 is defined as the width for this plot.

sections defined as

$$\langle\sigma(k)\rangle=\int_0^{35}[\sigma(\gamma,\mathrm{Tot})/k]dk. \quad (7)$$

These harmonic mean cross sections were used in turn to evaluate a harmonic mean energy defined by

$$\langle k\rangle=\int_0^{35}\sigma(\gamma,\mathrm{Tot})dk\Big/\int_0^{35}\sigma(\gamma,\mathrm{Tot})/kdk. \quad (8)$$

These energies are plotted in Fig. 33 and listed in Table III. Median energies as well as energies below which lie 25 and 75% of the classical sum rule integrated cross section are also plotted on Fig. 33. These forms of presenting the data are used in lieu of a plot of the location of the peak cross section because with either multi-peaked cross sections as found in silicon and oxygen, or very broad peaks as found in sodium and beryllium, the location in energy of the single highest cross section is a poor description of the cross-section shape. The parameters plotted show the definite trend to peak cross sections located at lower energies as Z is increased.

5. Giant-Resonance Width

No single definition of the width of the giant resonance has been found satisfactory for the variety of giant-resonance shapes found in the present experiment. Therefore, in order to provide a definition that would eliminate the experimenter's bias, the width was measured by the difference in energies listed in Table III at which 25 and 75% of the classical photonuclear sum rule occur. These values are plotted in Fig. 34. Two observations to be made from this figure are that the giant-resonance width, excepting beryllium with an atomic number of 4, is particularly wide near an atomic number of 11 (sodium) and that the sodium peak in the width curve is similar to the peak in a quadrupole-moment plot given by Gove.[42,43]

ACKNOWLEDGMENTS

The results reported in this paper are the product of several years of work on many important and tangent efforts on x-ray spectrometer developments, bremsstrahlung and pair-production theoretical studies, and synchrotron energy controls. Consequently, many persons have contributed their time and interests. The present authors wish to acknowledge particularly the help of Dr. R. Schrack who was of critical importance in supplying advice on the programming and general analysis problems, and of Dr. J. Leiss who was helpful in controlling and calibrating the operation of the synchrotron, as well as in providing constructive comments during the course of this experiment. We appreciate the critical reading of this manuscript by Dr. E. Hayward and Dr. E. G. Fuller.

APPENDIX: LEVEL-WIDTH CRITERIA

The use of long attenuators as in the present experiment naturally raises questions regarding the influences on the measured, transmitted, x-ray spectrum of saturation due to narrow nuclear levels.

In order to develop criteria on the influence of level widths, a calculation has been made of $I_0\Gamma_{\mathrm{eff}}$, the number of x rays removed by nuclear absorption from the spectrum.

Γ_{eff} is the effective level width, which can be evaluated from the following expression if Doppler broadening is neglected:

$$\Gamma_{\mathrm{eff}}=\int_{-\infty}^{+\infty}[1-e^{-\sigma_a(k)Nx}]d(k-k_0), \quad (A1)$$

where $\sigma_a(k)$ is the absorption cross section

$$\sigma_a(k)=\frac{\pi}{2}\lambda\!\!\!^{-2}\left(\frac{2J+1}{2I+1}\right)\frac{\Gamma\Gamma_\gamma}{(k-k_0)^2+\Gamma^2/4}\ \mathrm{cm}^2; \quad (A2)$$

$$\int\sigma_a(k)dk=\frac{\pi}{\Gamma}\left[\pi\lambda\!\!\!^{-2}\left(\frac{2J+1}{2I+1}\right)\Gamma\Gamma_\gamma\right]\ \mathrm{eV\ cm}^2, \quad (A3)$$

where k_0=resonance energy in MeV, k=x-ray photon energy in MeV, Γ=total width for the nuclear level in eV, Γ_γ=radiation width for the nuclear level in eV, $\lambda\!\!\!^{-}=1.95\times10^{-11}/k(\mathrm{MeV})$ cm, N=atoms/cc, and x=attenuator length in cm.

The integral in equation (A1) can be solved explicitly in Bessel functions as done by Dardel and Persson[44] or can be solved for two special cases in series expansions[45] in the variable, t, where

$$t=2\pi\lambda\!\!\!^{-2}\left(\frac{2J+1}{2I+1}\right)\frac{\Gamma_\gamma}{\Gamma}Nx. \quad (A4)$$

[42] H. E. Gove, *Proceedings of the International Conference on Nuclear Structure*, edited by D. A. Bromley and E. W. Vogt (University of Toronto Press, Toronto, 1960), p. 438.

[43] We are indebted to Dr. E. Hayward for pointing out the significant systematic variation with Z in the width of the giant resonance.

[44] G. V. Dardel and R. Persson, Nature **170**, 1117 (1952).

[45] M. Abramowitz (private communication).

When $t \ll 1$,

$$\Gamma_{\text{eff}} = \tfrac{1}{2}\Gamma\pi[t - \tfrac{1}{2}(t^2/2!) + (3t^3/8\cdot 3!) + \cdots] \quad \text{(A5)}$$

or, to a first approximation,

$$\Gamma_{\text{eff}} = (\Gamma\pi t/2). \quad \text{(A6)}$$

When $t \gg 1$,

$$\Gamma_{\text{eff}} = \tfrac{1}{2}\Gamma\pi[2(t/\pi)^{1/2} - \tfrac{1}{2}1/(\pi t)^{1/2} - 3/16(\pi t^3)^{1/2} + \cdots] \quad \text{(A7)}$$

or, to a first approximation,

$$\Gamma_{\text{eff}} = \Gamma(\pi t)^{1/2}. \quad \text{(A8)}$$

Since

$$t = \frac{2Nx}{\pi\Gamma}\int \sigma_a(k)dk, \quad \text{(A9)}$$

Eq. (A6) becomes

$$\Gamma_{\text{eff}} = Nx\int \sigma_a(k)dk \quad \text{for} \quad t \ll 1, \quad \text{(A10)}$$

and Eq. (A8) becomes

$$\Gamma_{\text{eff}} = \left(2Nx\Gamma\int \sigma_a(k)dk\right)^{1/2} \quad \text{for} \quad t \gg 1. \quad \text{(A11)}$$

Thus, in order to insure a good measurement of the integrated absorption cross section for a single level, the quantity t must be $\ll 1$.

This criterion in turn requires that

$$\frac{\Gamma_\gamma}{\Gamma} \ll \left(\frac{2I+1}{2J+1}\right)\frac{1}{2\pi\lambda^2 Nx} \quad \text{(A12)}$$

or, after making the appropriate substitutions and assuming the nuclear spin $I=0$ and dipole radiation $(J=1)$,

$$\Gamma_\gamma/\Gamma \ll Ak^2/4340\rho x, \quad \text{(A13)}$$

where ρx = attenuator length in g/cm^2 and A = atomic weight of the absorber.

In addition, Wilkinson[46] has shown that for light elements ($A \leq 20$) and electric-dipole transitions,

$$\Gamma_\gamma = 0.045\times 6.8\times 10^{-2} A^{2/3}k^3 = 3.06\times 10^{-4} A^{2/3}k^3. \quad \text{(A14)}$$

Thus Eq. (A13) becomes

$$\Gamma \gg 1.33(\rho x)(k/A^{1/3}) \text{ eV}. \quad \text{(A15)}$$

To be more specific, for a carbon attenuator, $k = 22.5$ MeV, $A = 12$, and $\rho x = 500$ g/cm^2. Thus

$$\Gamma \gg 6.5 \text{ keV}. \quad \text{(A16)}$$

Although there are not enough data[47] available to state specifically that all levels were sufficiently broad in the present experiment, it is probably a good assumption and has been assumed in the interpretation of the experimental data.

[46] D. H. Wilkinson, *Nuclear Spectroscopy*, edited by F. Ajzenberg-Selove (Academic Press Inc., New York, 1960), Part B, p. 859.

[47] Note should be made of the recent complete listing of Γ_n, Γ_p, and Γ_γ for various levels in O^{16} as given in K. N. Geller and E. G. Muirhead, Phys. Rev. Letters **2**, 371 (1963).